Journal of Solid State Chemistry **152,** 560–567 (2000)
doi:10.1006/jssc.2000.8731, available online at http://www.idealibrary.com on IDEAL®

Indides $LnNiIn_2$ (Ln = Pr, Nd, Sm) and Ferromagnetic PrRhIn

Vasyl' I. Zaremba,* Yaroslav M. Kalychak,* Vitaliy P. Dubenskiy,*
Rolf-Dieter Hoffmann,† and Rainer Pöttgen†,[1,2]

*Inorganic Chemistry Department, Ivan Franko National University of Lviv, Kyryla and Mephodiya Street 6, 79005 Lviv, Ukraine; and
†Anorganisch-Chemisches Institut, Universität Münster, Wilhelm-Klemm-Strasse 8, D-48149 Münster, Germany

Received January 20, 2000; in revised form March 20, 2000; accepted March 27, 2000

The title compounds were synthesized by reacting the elements in an arc-melting apparatus under purified argon and subsequent annealing at 970 K. The nickel containing compounds crystallize with a new structure type which was determined for $PrNiIn_2$: $Cmcm$, $a = 440.0(2)$ pm, $b = 1833.9(6)$ pm, $c = 2164.6(5)$ pm, w$R_2 = 0.0550$, 1451 F^2 values, and 66 parameters. From a geometrical point of view, the structure of $PrNiIn_2$ may be described as an intergrowth of small distorted $CaCu_5$-, CsCl-, and Cu_3Au-related slabs. The structure is also related to the $MgCuAl_2$ type by chemical twinning. The shortest interatomic distances within the $PrNiIn_2$ structure occur for the Ni–In and In–In contacts. The nickel and indium atoms form a three-dimensional $[NiIn_2]$ polyanion in which the praseodymium atoms fill distorted pentagonal channels. To a first approximation the formula may be written as $Pr^{3+}[NiIn_2]^{3-}$. PrRhIn adopts the ZrNiAl type structure: $P\bar{6}2m$, $a = 755.6(2)$ pm, $c = 404.8(1)$ pm, w$R_2 = 0.0285$, 361 F^2 values, and 14 parameters. Structural motifs of PrRhIn are tricapped trigonal prisms $[Rh1In_6Pr_3]$ and $[Rh2Pr_6In_3]$. The rhodium and indium atoms form a three-dimensional [RhIn] polyanion in which the praseodymium atoms are located in distorted hexagonal channels. Susceptibility measurements reveal Curie–Weiss behavior with a magnetic moment of 3.69(5) μ_B/Pr. PrRhIn orders ferromagnetically at $T_C = 5.8(6)$ K and shows a saturation magnetization of 1.60(5) μ_B/Pr at 2 K and 5.5 T. Resistivity measurements indicate metallic behavior with a specific resistivity of 105 ± 20 μΩ cm at room temperature.

INTRODUCTION

The ternary systems rare earth metal–nickel–indium have intensively been investigated in recent years (1). These studies resulted in the syntheses of more than a hundred ternary compounds with peculiar crystal structures and largely varying physical properties (2). The various structures of these indium compounds have briefly been reviewed by Kalychak (3).

Recently, the structures and physical properties of the indides $Ln_5Ni_6In_{11}$ (Ln = La, Ce, Pr, Nd) have been reported (4–6). These structures are built up from a complex three-dimensional $[Ni_6In_{11}]$ tubular polyanionic network in which the rare earth atoms occupy distorted pentagonal and hexagonal channels. Within the $[Ni_6In_{11}]$ polyanions short Ni–Ni, Ni–In, and In–In distances are indicative for strongly bonding Ni–Ni, Ni–In, and In–In interactions. We have now successfully synthesized the indides $LnNiIn_2$ (Ln = Pr, Nd, Sm). Their composition is very close to that of $Ln_5Ni_6In_{11}$, but they form a significantly different polyanionic network in which no Ni–Ni contacts occur.

Herein we report on the syntheses and structure refinements of these new compounds. Additionally we determined the structure and some physical properties of PrRhIn. Excerpts of this work have been presented recently at a conference (7).

EXPERIMENTAL PROCEDURES

Starting materials for the synthesis of $PrNiIn_2$, $NdNiIn_2$, $SmNiIn_2$, and PrRhIn were sublimed ingots of the rare earth elements (Johnson Matthey), nickel wire (Johnson Matthey, ∅ 0.38 mm), rhodium powder (Degussa, 200 mesh), and indium tear drops (Johnson Matthey), all with stated purities greater than 99.9%. The large rare earth ingots were initially cut into smaller pieces under paraffin oil. The latter was washed off with *n*-hexane. Both liquids were dried over sodium wire. The rare earth pieces were kept in Schlenk tubes under argon.

In a first step, the small rare earth pieces were arc-melted to buttons under argon. The argon was purified before over titanium sponge (900 K), silica gel, and molecular sieves. The pre-melting procedure strongly reduces scattering of these elements during the exothermic reactions with the other elements. The rhodium powder was pressed to small pellets (∅ 6 mm).

[1] To whom correspondence should be addressed.

[2] Present address: Prof. Dr. Rainer Pöttgen, Department Chemie, Ludwig-Maximilians-Universität München, Butenandtstrasse 5-13 (Haus D), 81377 Munich, Germany. E-mail: rapch@cup.uni-muenchen.de.

0022-4596/00 $35.00

TABLE 1
Lattice Constants of Orthorhombic Indides LnNiIn$_2$ (Ln = Pr, Nd, Sm) and Hexagonal PrRhIn

Compound	a (pm)	b (pm)	c (pm)	V (nm^3)
PrNiIn$_2$	440.0(2)	1833.9(6)	2164.6(5)	1.7467
NdNiIn$_2$	438.0(1)	1833.5(4)	2151.6(5)	1.7279
SmNiIn$_2$	434.9(2)	1818.4(6)	2143.6(7)	1.6952
PrRhIn	755.6(2)	a	404.8(1)	0.2001

The rare earth buttons (about 300 mg) were mixed with the nickel wire, the rhodium pellet, and the indium tear drops in the ideal 1:1:2 or 1:1:1 atomic ratios and arc-melted under an argon atmosphere of about 800 mbar. The buttons were remelted at least three times to ensure homogeneity. The total weight losses after the melting procedures were always smaller than 0.5 wt%. The compact polycrystalline samples were subsequently sealed in evacuated quartz glass ampoules and annealed at 970 K for two weeks.

The products were characterized through their X-ray powder patterns (Dron–4.07 powder diffractometer, Fe$K\alpha$ radiation) using 5N silicon (a = 543.07 pm) as an internal standard. The patterns of the nickel compounds could completely be indexed with C-centered orthorhombic cells, while the PrRhIn pattern showed a hexagonal cell. The lattice constants (see Table 1) were obtained from least-squares fits of the X-ray powder data. To assure correct indexing, the observed patterns were compared with calculated ones (8) taking the atomic positions from the structure refinements. The lattice constants of the PrNiIn$_2$ and PrRhIn single crystals were in good agreement with those derived from the powder data.

Single crystal intensity data were collected at room temperature by use of a four-circle diffractometer (CAD4) with graphite monochromatized Mo$K\alpha$ (71.073 pm) radiation and a scintillation counter with pulse height discrimination. The scans were taken in the $\omega/2\theta$ mode and an empirical absorption correction was applied on the basis of ψ-scan data.

The magnetic susceptibilities of polycrystalline pieces of PrRhIn were measured with a SQUID magnetometer (MPMS, Quantum Design, Inc.) between 2 and 300 K with magnetic flux densities up to 5.5 T. Resistivity measurements were performed with a conventional four-point technique. Four copper filaments were glued to the irregularly shaped samples (typical dimensions $1 \times 1 \times 1$ mm^3) using a well conducting silver epoxy paste. Cooling and heating curves were identical within the error limits.

RESULTS AND DISCUSSION

Structure Refinements

Irregularly shaped single crystals of PrNiIn$_2$ and PrRhIn were isolated from the annealed samples and examined by use of a Buerger camera. The reciprocal layers $hk0$ and $hk1$ of PrRhIn showed the hexagonal Laue class $6/mmm$ and no systematic extinctions. The non-centrosymmetric group $P\bar{6}2m$ was found to be correct during the structure refinements, in agreement with our previous results on isotypic YbPtSn (9). The precession photographs of PrNiIn$_2$ (reciprocal layers $hk0$ and $hk1$) showed the orthorhombic Laue class mmm and the systematic extinctions were compatible with space group $Cmcm$ (No. 63). All relevant crystallographic data and experimental details for the data collections are listed in Table 2.

TABLE 2
Crystal Data and Structure Refinement for PrNiIn$_2$ and PrRhIn

Empirical formula	PrNiIn$_2$	PrRhIn
Molar mass (g/mol)	429.26	358.64
Space group, Z	$Cmcm$, 20	$P\bar{6}2m$, 3
Pearson symbol	oC80	hP9
Unit cell dimensions	Table 1	Table 1
Calculated density (g/cm^3)	8.16	8.93
Crystal size (μm^3)	$45 \times 55 \times 65$	$20 \times 20 \times 30$
Transmission ratio (max/min)	2.27	1.27
Absorption coefficient (mm^{-1})	31.8	32.3
F(000)	3700	459
θ range for data collection	2° to 30°	2° to 35°
Range in hkl	±6, ±25, ±30	±12, ±12, ±6
Total no. of reflections	5825	2070
No. of independent reflections	1451 (R_{int} = 0.0289)	361 (R_{int} = 0.0332)
No. of reflections with $I > 2\sigma(I)$	1280 (R_{sigma} = 0.0220)	345 (R_{sigma} = 0.0178)
No. of data/restraints/parameters	1451/0/66	361/0/14
Goodness-of-fit on F^2	1.137	1.141
Final R indices [$I > 2\sigma(I)$]	R_1 = 0.0215	R_1 = 0.0127
	wR_2 = 0.0507	wR_2 = 0.0273
R indices (all data)	R_1 = 0.0274	R_1 = 0.0147
	wR_2 = 0.0550	wR_2 = 0.0285
Extinction coefficient	0.00057(2)	0.0065(4)
Flack parameter	—	−0.01(2)
Largest diff. peak and hole (e/Å^3)	2.28 and −2.33	1.00 and −1.04

The atomic parameters of YbPtSn (9) were taken as starting values for PrRhIn, while those for PrNiIn$_2$ were deduced from an automatic interpretation of direct methods with Shelxs-97 (10). Both structures were then successfully refined using Shelxl-97 (11) (full-matrix least-squares on F^2) with anisotropic atomic displacement parameters for all atoms. As a check for the correct composition and the correct site assignment the occupancy parameters of both compounds were refined in a separate series of least-squares cycles along with the displacement parameters. All sites were fully occupied within two standard deviations, and in the final cycles the ideal occupancy parameters were assumed again. Final difference Fourier syntheses were flat (Table 2). The positional parameters and interatomic distances of the refinements are listed in Tables 3 and 4. Listings of the observed and calculated structure factors are available.[3]

[3] Details may be obtained from Fachinformationszentrum Karlsruhe, D-76344 Eggenstein-Leopoldshafen, Germany, by quoting the Registry Nos. CSD-411077 (PrNiIn$_2$) and CSD-411076 (PrRhIn).

TABLE 3
Atomic Coordinates and Isotropic Displacement Parameters (pm^2) for $PrNiIn_2$ and PrRhIn

Atom	Wyckoff site	x	y	z	U_{eq}[a]
		$PrNiIn_2$ (space group *Cmcm*)			
Pr1	8*f*	0	0.43744(2)	0.42014(2)	87(1)
Pr2	8*f*	0	0.22883(2)	0.37236(2)	78(1)
Pr3	4*c*	0	0.46930(3)	$\frac{1}{4}$	79(1)
Ni1	8*f*	0	0.34429(5)	0.53222(5)	95(2)
Ni2	8*f*	0	0.01428(5)	0.34209(5)	97(2)
Ni3	4*c*	0	0.31569(8)	$\frac{1}{4}$	133(3)
In1	4*c*	0	0.72458(4)	$\frac{1}{4}$	102(2)
In2	8*f*	0	0.80026(3)	0.46677(2)	83(1)
In3	8*f*	0	0.59918(3)	0.35617(2)	82(1)
In4	8*f*	0	0.86365(3)	0.32482(2)	93(1)
In5	4*c*	0	0.10966(4)	$\frac{1}{4}$	105(2)
In6	8*f*	0	0.06702(3)	0.45704(2)	79(1)
		PrRhIn (space group $P\bar{6}2m$)			
Pr	3*g*	0.58866(5)	0	$\frac{1}{2}$	93(1)
Rh1	1*b*	0	0	$\frac{1}{2}$	119(2)
Rh2	2*c*	1/3	2/3	0	112(1)
In	3*f*	0.24905(6)	0	0	96(1)

[a] U_{eq} is defined as one-third of the trace of the orthogonalized $\mathbf{U}_{ij}$ tensor.

TABLE 4
Interatomic Distances (pm), Calculated with the Lattice Constants taken from X-ray Powder Data of $PrNiIn_2$ and PrRhIn

	$PrNiIn_2$		
Pr1:	1 Ni1 296.7	Ni2: 1 In5 265.2	In3: 1 Ni1 262.9
	2 Ni2 311.1	1 In6 267.0	2 Ni2 271.2
	1 In3 327.4	2 In3 271.2	2 In6 315.5
	2 In4 330.6	1 In4 278.8	2 In5 318.7
	2 In6 333.6	2 Pr3 308.1	1 In1 325.1
	2 In6 345.2	2 Pr1 311.1	2 Pr2 325.8
	2 In2 349.1		1 Pr1 327.4
	1 Pr3 372.9	Ni3: 2 In1 276.3	1 Pr3 331.0
	1 Pr2 396.3	1 Pr3 281.7	
		4 In4 287.0	In4: 1 Ni2 278.8
Pr2:	1 Ni3 309.1	2 Pr2 309.1	2 Ni3 287.0
	2 In3 325.8		1 In1 302.1
	2 In2 327.6	In1: 2 Ni3 276.3	1 In4 323.9
	2 Ni1 330.2	2 In4 302.1	1 In2 328.5
	1 In5 343.4	2 In5 304.7	2 Pr1 330.6
	2 In1 344.4	2 In3 325.1	2 Pr3 334.9
	2 In4 346.6	4 Pr2 344.4	2 Pr2 346.6
	1 In6 348.8		
	1 In2 352.3	In2: 1 Ni1 265.1	In5: 2 Ni2 265.2
	1 Pr1 396.3	2 Ni1 273.8	2 In1 304.7
		1 In6 294.0	4 In3 318.7
Pr3:	1 Ni3 281.7	2 In2 321.0	2 Pr3 338.6
	4 Ni2 308.1	2 Pr2 327.6	2 Pr2 343.4
	2 In3 331.0	1 In4 328.5	
	4 In4 334.9	2 Pr1 349.1	In6: 1 Ni2 267.0
	2 In5 338.6	1 Pr2 352.3	2 Ni1 274.6
	2 Pr1 372.9		1 In2 294.0
			1 In6 308.3
Ni1:	1 In3 262.9		2 In3 315.5
	1 In2 265.1		2 Pr1 333.5
	2 In2 273.8		2 Pr1 345.2
	2 In6 274.6		1 Pr2 348.8
	1 Pr1 296.7		
	2 Pr2 330.2		
		PrRhIn	
Pr:	4 Rh2 305.0	Rh1: 6 In 276.4	In: 2 Rh1 276.4
	1 Rh1 310.8	3 Pr 310.8	2 Rh2 289.0
	2 In 326.8		2 In 325.9
	4 In 338.4	Rh2: 3 In 289.0	2 Pr 326.8
	4 Pr 395.2	6 Pr 305.0	4 Pr 338.4
	2 Pr 404.8		

Note. All distances within the first coordination spheres are listed. Standard deviations are all equal to or less than 0.2 pm.

Crystal Chemistry and Chemical Bonding

Three new ternary compounds, $PrNiIn_2$, $NdNiIn_2$, and $SmNiIn_2$, have been synthesized in the ternary systems rare earth metal–nickel–indium. In these ternary systems the largest number of ternary compounds by far has been observed. Up to now about 120 ternary indides have been reported (3). It is worthwhile to note that various compounds with quite similar compositions have been observed in these ternary systems, i.e., $Ln_5Ni_6In_{11}$ (Ln = La–Nd) with $Pr_5Ni_6In_{11}$-type structure (4–6), $LnNiIn_2$ (Ln = Eu–Dy) with $MgCuAl_2$-type structure (12, 13), and $Ln_{10}Ni_9In_{20}$ (Ln = Ho, Er, Tm, Lu) with $Ho_{10}Ni_9In_{20}$-type structure (14). The three structure types have only a small range of stability within the rare earth series, indicating that the formation of the respective structure type most likely depends on the size of the rare earth atom.

The $PrNiIn_2$ structure seems relatively complex with 12 crystallographically independent sites and 80 atoms within the unit cell. From a geometrical point of view, the $PrNiIn_2$ structure may be described as an intergrowth of distorted $CaCu_5$ (different ternary compositions), CsCl, and Cu_3Au related slabs as outlined in Fig. 1. These structural features are frequently observed for such intermetallic compounds (3, 15). The structure of $Pr_5Ni_6In_{11}$ has very similar slabs, i.e., $CeMg_2Si_2$, Cu_3Au, CsCl, and $CaCu_5$. The fragments, however, constitute a different tiling when compared with $PrNiIn_2$.

A closer look at the nickel–indium network of $PrNiIn_2$ reveals that larger fragments of this structure resemble the $MgCuAl_2$-type structure (16) of $GdNiIn_2$ (12). This structural relationship is emphasized in Fig. 2, where the $MgCuAl_2$ slabs are shaded. According to the concepts of Andersson (17) and Parthé (18–21), the $PrNiIn_2$ structure may be described as a chemical twinning or an intergrowth of $MgCuAl_2$ slabs. These slabs are connected at the mirror planes at $xy\frac{1}{4}$ and $xy\frac{3}{4}$. The praseodymium atoms are

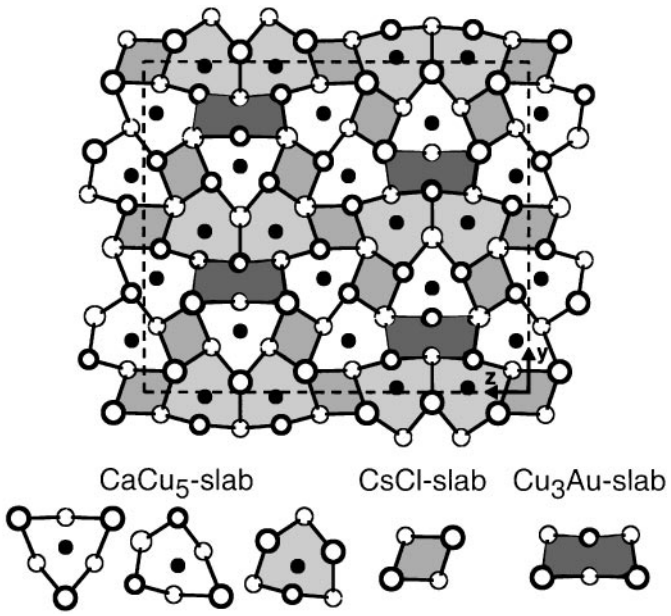

FIG. 1. Projection of the $PrNiIn_2$ structure onto the yz plane. All atoms lie on mirror planes at $x = 0$ (thin lines) and $x = \frac{1}{2}$ (thick lines). Praseodymium, nickel, and indium atoms are drawn as large open, filled, and medium open circles, respectively. The distorted $CaCu_5$-, CsCl-, and Cu_3Au-related slabs are emphasized.

most likely too large to favor a $MgCuAl_2$-type structure as $GdNiIn_2$ (12) does. Nevertheless, smaller fragments clearly resemble the $GdNiIn_2$ structure and the geometrical frustration is solved by the chemical twinning, leading to the optimal energetic solution for this atomic arrangement.

Three crystallographically different praseodymium sites occur in the $PrNiIn_2$ structure. These praseodymium atoms have high coordination numbers (CN), i.e., CN14 (2 Pr + 3 Ni + 9 In) for Pr1, CN15 (1 Pr + 3 Ni + 11 In) for Pr2, and CN15 (2 Pr + 5 Ni + 8 In) for Pr3. The most remarkable features of the praseodymium coordinations are the relatively short Pr3–Ni3 and Pr1–Ni1 distances at 282 and 297 pm, respectively. These Pr–Ni distances, by far the shortest in the structure of $PrNiIn_2$, are only slightly larger than the sum of the metallic single-bond radii of 280 pm for praseodymium and nickel (22). Similar short rare earth metal–nickel distances occur also in the structures of $Nd_5Ni_6In_{11}$ (6) (Nd1–Ni1, 286 pm), $Sm_{12}Ni_6In$ (23) (Sm–Ni, 266 pm), and $Lu_5Ni_2In_4$ (24) (Lu3–Ni, 275 pm). The Pr3 site lies on the mirror planes at $xy\frac{1}{4}$ and $xy\frac{3}{4}$, where the chemical twinning occurs. This site has the largest number of nickel neighbors.

The three nickel sites have CN9 with indium and praseodymium atoms in their coordination shell. In contrast to the structure of $Nd_5Ni_6In_{11}$ (6), no Ni–Ni contacts occur in $PrNiIn_2$. The various Ni–In distances range from 263 to 287 pm. The shorter distances compare well with the sum of Pauling's single-bond radii (22) of 265 pm for nickel and indium. The six crystallographically different indium atoms have CN12 with praseodymium, nickel, and indium neighbors. Each indium atom has at least three indium neighbors at In–In distances ranging from 294 to 329 pm. Most In–In distances are significantly shorter than in elemental indium (tetragonally distorted fcc variant), where each indium atom has four neighbors at 325 pm and eight additional neighbors at 338 pm (25). The comparison of the interatomic distances clearly shows that Ni–In and In–In

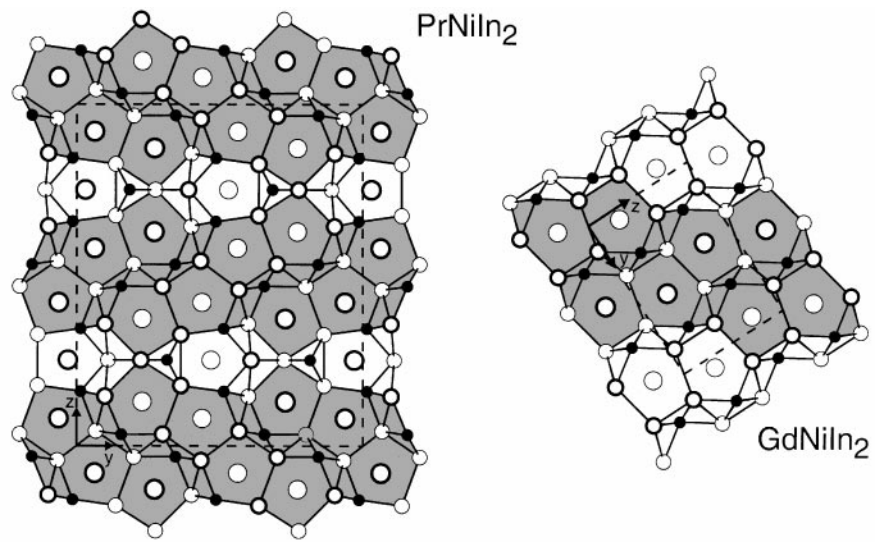

FIG. 2. $MgCuAl_2$ related slabs in the structures of the $PrNiIn_2$ and $GdNiIn_2$. All atoms lie on mirror planes at $x = 0$ (thin lines) and $x = \frac{1}{2}$ (thick lines). Praseodymium (gadolinium), nickel, and indium atoms are drawn as large open, filled, and medium open circles, respectively.

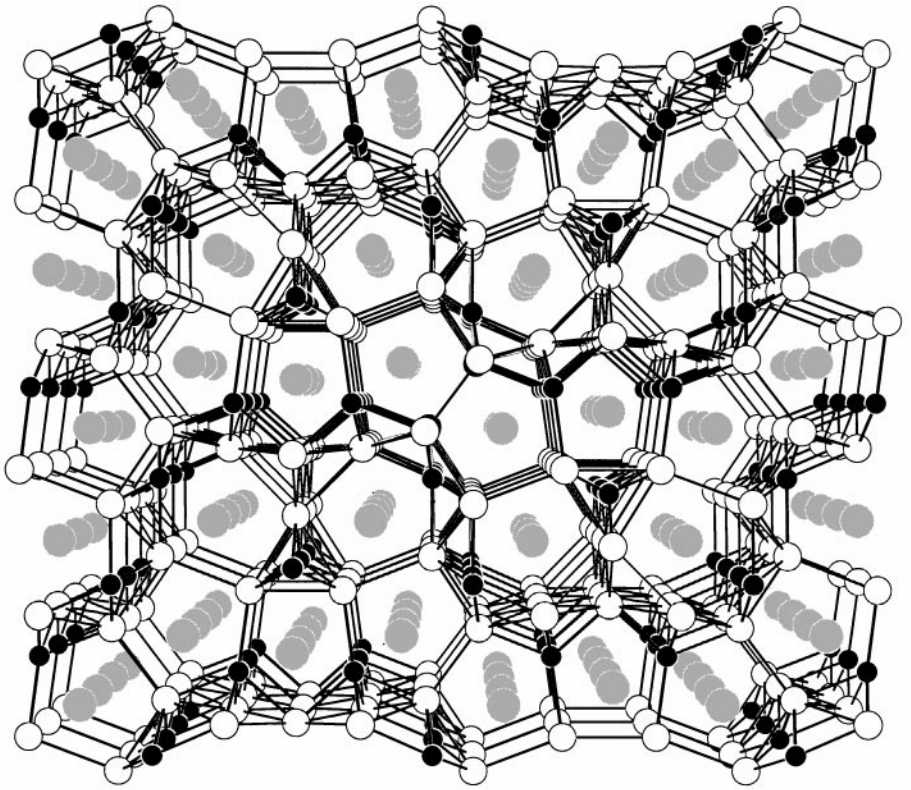

FIG. 3. Perspective view of the $PrNiIn_2$ structure along the x axis. The three-dimensional $[NiIn_2]$ polyanion is emphasized. Praseodymium, nickel, and indium atoms are drawn as gray, black, and open circles, respectively.

bonding (most likely of covalent character) play an important role in the structure of $PrNiIn_2$.

Apart from the geometric description of $PrNiIn_2$ by an intergrowth of $CaCu_5$-, CsCl-, and Cu_3Au-related slabs, we favor a description by the concept of polyanionic networks. The praseodymium atoms as the most electropositive component of the compound (Pauling's electronegativities (26) are 1.1 for Pr, 1.8 for Ni, and 1.7 for In) have largely transferred their valence electrons to the $[NiIn_2]$ network. To a first approximation, the formula may be written as $Pr^{3+}[NiIn_2]^{3-}$ emphasizing the covalent Ni–In and In–In bonding within the polyanion. A cutout of the complex three-dimensionally infinite $[NiIn_2]$ polyanion is presented in Fig. 3. Such complex polyanions with similar bonding characteristic also occur in structures as $CeNiIn_4$ (27), $Nd_5Ni_6In_{11}$ (6), $CaAuIn_2$ (28), or $Ca_2Au_3In_4$ (29). Although the description by a polyanionic network seems adequate at first sight, some words of caution seem to be appropriate, since bonding interactions also occur between the praseodymium and nickel(indium) atoms (see shortest distances in Table 3; Pr3–Ni3, 282 pm; Pr1–In3, 327 pm), indicating mixing of praseodymium and nickel(indium)-centered bands. This is also true for $Nd_5Ni_6In_{11}$ (6), $Sr_2Pt_3In_4$ (29), and $CaAuIn_2$ (28). A TB-LMTO-ASA band structure calculation of $CaAuIn_2$ clearly showed interactions between the calcium atoms and the neighboring gold and indium atoms within the three-dimensional $[AuIn_2]$ polyanion.

Equiatomic PrRhIn adopts the ZrNiAl-type structure (30–32), a ternary ordered version of the well-known Fe_2P type (33). A projection and a perspective view of this structure are shown in Fig. 4. From a geometrical point of view, the building elements are two types of tri-capped, rhodium-centered trigonal prisms. The Rh1 atoms are located within trigonal prisms of six indium atoms which are capped by praseodymium atoms. For Rh2 the prisms are formed by the praseodymium atoms and capped by the indium atoms. Six Rh2-centered prisms form rings via common praseodymium edges (upper part of Fig. 3). The Rh1-centered prisms are located within these rings.

The shortest interatomic distances in PrRhIn occur between the rhodium and indium atoms. The Rh1–In and Rh2–In distances range from 276 to 289 pm. They are only slightly larger than the sum of Pauling's single bond radii of 275 pm for rhodium and indium (22). Similar Rh–In contacts have recently also been observed in binary $RhIn_3$ (264–275 pm) (34), and in the ternary indides EuRhIn (277–279 pm) (35), $CaRhIn_2$ (271–280) (36), and $SrRhIn_2$

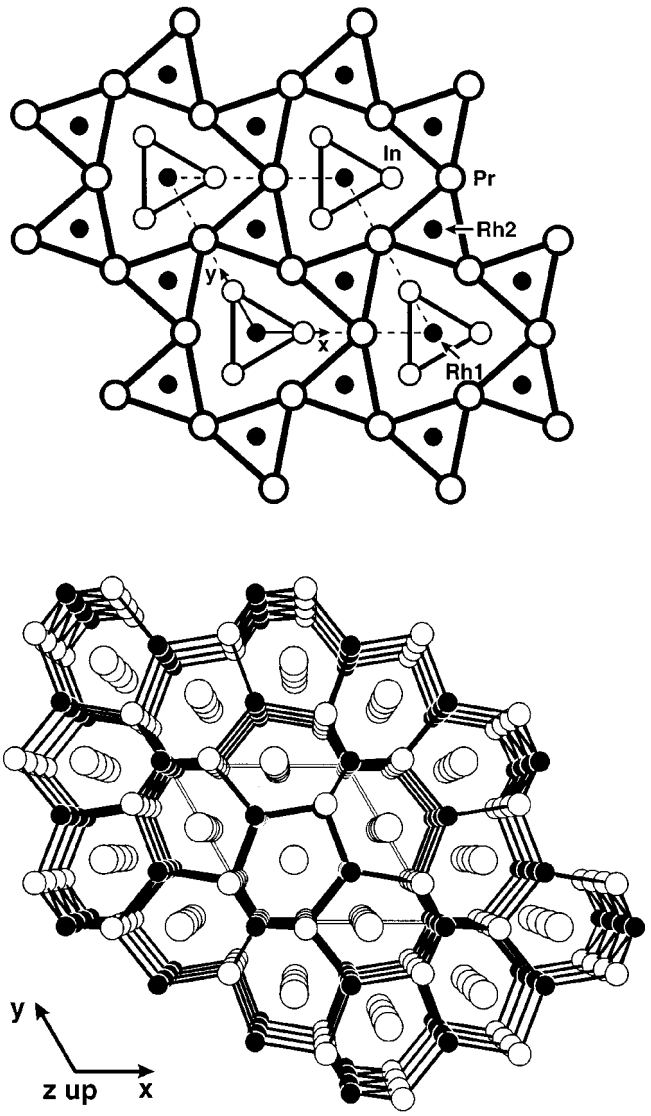

FIG. 4. Projection (upper part) and perspective view (lower part) of the PrRhIn structure. In the upper part of the drawing the rhodium-centered trigonal prisms are emphasized, while the three-dimensional infinite [RhIn] polyanion is shown in the lower part. The praseodymium, rhodium, and indium atoms are drawn as large open, filled, and medium open circles, respectively.

(278–279 pm) (37). The In–In distances of 326 pm within the triangular faces of the trigonal prisms at the origin compare well with the shortest In–In distances of 325 pm in elemental indium (25). Considering the strong Rh–In and In–In interactions, PrRhIn can be described by a most likely covalently bonded three-dimensional [RhIn] polyanionic network as outlined in Fig. 4. According to the magnetic susceptibility investigation (see below), the praseodymium atoms in PrRhIn are in the trivalent oxidation state. The formula of PrRhIn may thus, to a first approximation, be written as $Pr^{3+}[RhIn]^{3-}$, emphasizing a $[RhIn]^{3-}$ polyanion.

Magnetic and Electrical Properties of PrRhIn

The temperature dependence of the inverse magnetic susceptibility of PrRhIn is displayed in Fig. 5. PrRhIn shows Curie–Weiss behavior above 20 K; however, a slight convex curvature is observed, indicating a temperature-independent contribution. We have thus fit the data above 20 K with a modified Curie–Weiss expression $\chi = \chi_0 + C/(T - \Theta)$ resulting in a paramagnetic Curie temperature (Weiss constant) of $-2.7(4)$ K, an experimental magnetic moment of 3.69(5) μ_B/Pr, and a temperature-independent contribution χ_0 of $2.5(1) \times 10^{-9}$ m^3/mol. The experimental magnetic moment is close to the calculated value of 3.58 μ_B for the free Pr^{3+} ion (38). The temperature-independent contribution is in the order of magnitude of a Pauli paramagnet and most likely results from the conduction electrons of this metallic compound (see below).

Ferromagnetic ordering of the praseodymium magnetic moments is detected at low temperatures (insert of Fig. 5). The precise Curie temperature of $T_C = 5.8(6)$ K was determined from the derivative $d\chi/dT$ of a kink-point measurement (insert of Fig. 6) at a magnetic flux density of 0.002 T. The magnetization versus external magnetic field depence is linear at 50 K (Fig. 7), as expected for a paramagnetic material. At 2 K we observe a strong increase of the magnetization, even at very low field strengths. The magnetization curve shows only a very small hysteresis with negligible coercivity and remanent magnetization, classifying PrRhIn as a very soft ferromagnet. At the highest obtainable magnetic field of 5.5 T the magnetization amounts to 1.60(5) μ_B/Pr, significantly reduced when compared with the maximal value of 3.20 μ_B/Pr according to $g \times J$ (2). The

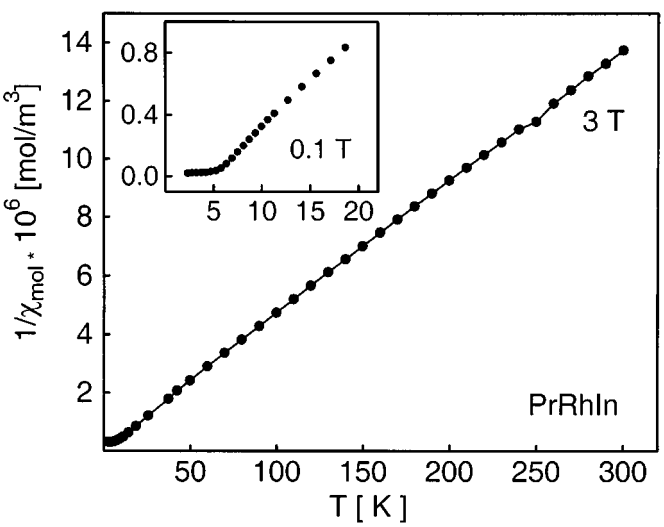

FIG. 5. Temperature dependence of the reciprocal susceptibility of PrRhIn measured at an external field of 3 T. The low-temperature behavior is presented in the insert.

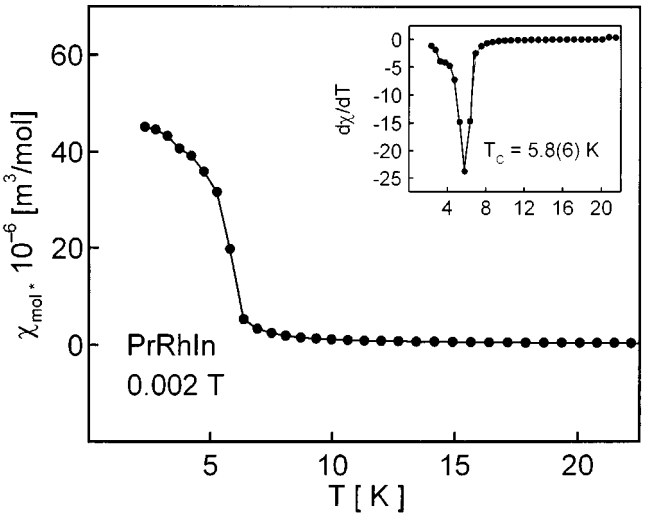

FIG. 6. Low-temperature susceptibility (field-cooling mode) of PrRhIn at 0.002 T (kink-point measurement). The insert shows the derivative $d\chi/dT$, which has a sharp peak at $T_C = 5.8(6)$ K.

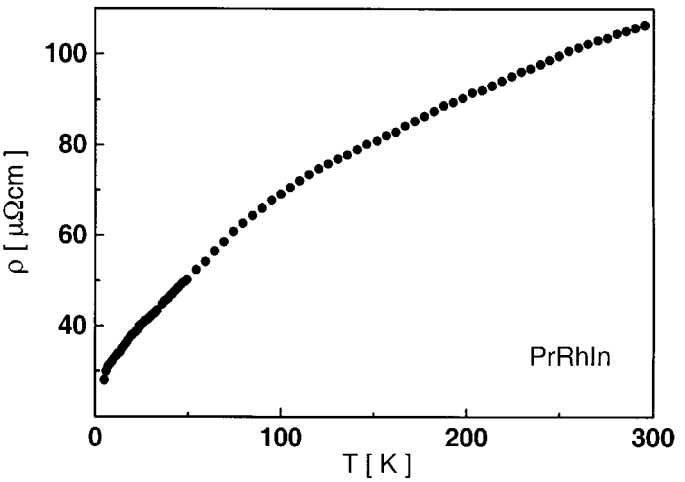

FIG. 8. Temperature dependence of the specific resistivity of PrRhIn.

reduced moment may be attributed to crystal field splitting. Similar reduced moments have also been observed for the ferromagnets $PrRu_2Ge_2$ (1.82 μ_B/Pr) (39), PrCuAl (1.30 μ_B/Pr) (40), and PrCuSi (2.02 μ_B/Pr) (41).

In Fig. 8 we present the temperature dependence of the specific resistivity of PrRhIn. The specific resistivity of 105 ± 20 μΩcm at room temperature decreases to 28 ± 10 μΩcm at 4.2 K as expected for a metallic material. The resistivity ratio $\rho(4.2\,\text{K})/\rho(300\,\text{K})$ is 0.27. The large error limits account for the different values obtained for several samples. The region of negative curvature near 100 K can most likely be attributed to crystal field effects and the small drop at 4.2 K is certainly due to spin–disorder freezing in the ferromagnetically ordered state.

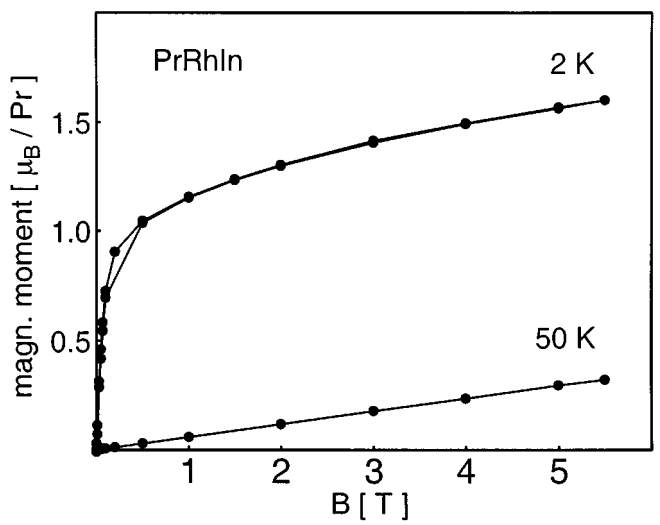

FIG. 7. Magnetic moment versus external magnetic flux density for PrRhIn at 2 and 50 K.

ACKNOWLEDGMENTS

We are grateful to Prof. W. Jeitschko for his interest and support. Special thanks go to Dipl.-Ing. U. Ch. Rodewald for the intensity data collections, to Dipl.-Chem. B. Künnen for the resistivity measurement, and to Dipl.-Chem. G. Kotzyba for the susceptibility measurements. This work was financially supported by the Fonds der Chemischen Industrie and the Deutsche Forschungsgemeinschaft.

REFERENCES

1. P. Villars and L. D. Calvert, "Pearson's Handbook of Crystallographic Data for Intermetallic Phases," 2nd ed. American Society for Metals, Materials Park, OH 44073, 1991. [and Desk Edition, 1997]
2. A. Szytula and J. Leciejewicz, "Handbook of Crystal Structures and Magnetic Properties of Rare Earth Intermetallics." CRC Press, Boca Raton, FL, 1994.
3. Ya. M. Kalychak, *J. Alloys Compd.* **262–263,** 341 (1997).
4. Ya. M. Kalychak, P. Yu. Zavalii, V. M. Baranyak, O. V. Dmytrakh, and O. I. Bodak, *Sov. Phys. Crystallogr.* **32,** 600 (1987); *Kristalografijya* **32,** 1021 (1987).
5. J. Tang, K. A. Gschneidner, Jr., S. J. White, M. R. Roser, T. J. Goodwin, and L. R. Corrucini, *Phys. Rev. B* **52,** 7328 (1995).
6. R. Pöttgen, R.-D. Hoffmann, R. K. Kremer, and W. Schnelle, *J. Solid State Chem.* **142,** 180 (1999).
7. V. I. Zaremba, Ya. V. Galadzhun, V. P. Dubenskiy, Ya. M. Kalychak, R.-D. Hoffmann, and R. Pöttgen, *Z. Kristallogr.* **Suppl. 17,** 123 (2000).
8. K. Yvon, W. Jeitschko, and E. Parthé, *J. Appl. Crystallogr.* **10,** 73 (1977).
9. R. Pöttgen, A. Lang, R.-D. Hoffmann, B. Künnen, G. Kotzyba, R. Müllmann, B. D. Mosel, and C. Rosenhahn, *Z. Kristallogr.* **214,** 143 (1999).
10. G. M. Sheldrick, "Shelxs-97, Program for the Solution of Crystal Structures." University of Gottingen, Gottigen, 1997.

11. G. M. Sheldrick, "Shelxl-97, Program for Crystal Structure Refinement." University of Gottingen, Gottingen, 1997.
12. V. I. Zaremba, O. Ya. Zakharko, Ya. M. Kalychak, and O. I. Bodak, *Dopov. Akad. Nauk. Ukr. RSR*, *Ser. B* (12) 44 (1987).
13. Ya. M. Kalychak and Ya. V. Galadzhun, *Z. Kristallogr.* **212,** 292 (1997).
14. V. I. Zaremba, V. K. Belsky, Ya. M. Kalychak, V. K. Pecharsky, and E. I. Gladyshevsky, *Dopov. Akad. Nauk. Ukr. RSR*, *Ser. B* (3) 45 (1987).
15. E. Parthé, L. Gelato, B. Chabot, M. Penzo, K. Cenzual, and R. E. Gladyshevskii, TYPIX—Standardized Data and Crystal Chemical Characterization of Inorganic Structure Types, *in* Gmelin Handbook of Inorganic and Organometallic Chemistry, 8th ed. Springer-Verlag, Berlin, 1993.
16. B. Aronsson, M. Bäckman, and S. Rundqvist, *Acta Chem. Scand.* **14,** 1001 (1960).
17. S. Andersson, *Angew. Chem.* **95,** 67 (1983).
18. E. Parthé and B. Chabot, *in* "Handbook on the Physics and Chemistry of Rare Earths," Vol. 6, p. 113, (K. A. Gschneidner, Jr., and L. Eyring, eds.). North-Holland, Amsterdam, 1984.
19. K. Cenzual and E. Parthé, *Acta Crystallogr. Sect. C* **40,** 1127 (1984).
20. E. Parthé, B. Chabot, and K. Cenzual, *Chimia* **39,** 164 (1985).
21. E. Parthé, "Elements of Inorganic Structural Chemistry." Pöge, Leipzig, 1990.
22. L. Pauling, "The Nature of the Chemical Bond and The Structures of Molecules and Crystals." Cornell University Press, Ithaca, NY, 1960.
23. Ya. M. Kalychak, V. I. Zaremba, A. Stepien'-Damm, Ya. V. Galadzhun, and L. G. Aksel'rud, *Crystallogr. Rep.* **43,** 12 (1998).
24. V. I. Zaremba, Ya. M. Kalychak, P. Yu. Zavalij, and V. A. Bruskov, *Kristallografiya* **36,** 1415 (1991).
25. J. Donohue, "The Structures of the Elements." Wiley, New York, 1974.
26. J. Emsley, "The Elements." Clarendon Press, Oxford, 1989.
27. R. Pöttgen, *J. Mater. Chem.* **5,** 769 (1995).
28. R.-D. Hoffmann, R. Pöttgen, G. A. Landrum, R. Dronskowski, B. Künnen, and G. Kotzyba, *Z. Anorg. Allg. Chem.* **625,** 789 (1999).
29. R.-D. Hoffmann and R. Pöttgen, *Z. Anorg. Allg. Chem.* **625,** 994 (1999).
30. P. I. Krypyakevich, V. Ya. Markiv, and E. V. Melnyk, *Dopov. Akad. Nauk. Ukr. RSR*, *Ser. A* 750 (1967).
31. A. E. Dwight, M. H. Mueller, R. A. Conner, Jr., J. W. Downey, and H. Knott, *Trans. Met. Soc. AIME* **242,** 2075 (1968).
32. M. F. Zumdick, R.-D. Hoffmann, and R. Pöttgen, *Z. Naturforsch. B* **54,** 45 (1999).
33. S. Rundqvist and F. Jellinek, *Acta Chem. Scand.* **13,** 425 (1959).
34. R. Pöttgen, R.-D. Hoffmann, and G. Kotzyba, *Z. Anorg. Allg. Chem.* **624,** 244 (1998).
35. R. Pöttgen, R.-D. Hoffmann, M. H. Möller, G. Kotzyba, B. Künnen, C. Rosenhahn, and B. D. Mosel, *J. Solid State Chem.* **145,** 174 (1999).
36. R.-D. Hoffmann and R. Pöttgen, *Z. Anorg. Allg. Chem.* **626,** 28 (2000).
37. R.-D. Hoffmann, U. Ch. Rodewald, and R. Pöttgen, *Z. Naturforsch. B* **54,** 38 (1999).
38. H. Lueken, "Magnetochemie." Teubner, Stuttgart, 1999.
39. I. Felner and I. Nowik, *J. Phys. Chem. Solids* **46,** 681 (1985).
40. H. Oesterreicher, *J. Less-Common Met.* **30,** 225 (1973).
41. H. Oesterreicher, *Phys. Stat. Sol. A* **34,** 723 (1976).